Materials for Renewable and Sustainable Energy (2024) 13:97–107
https://doi.org/10.1007/s40243-024-00256-9

ORIGINAL PAPER

Incorporation of multilayered double hydroxides/sepiolite augments proton conductivity performance in low sulfonated polyether sulfone octyl sulfonamide

khaled Charradi[1] · Walid Mabrouk[2] · Imen Ben Kacem[2,3] · Nizar Bellakhal[3] · Youssef O. Al-Ghamdi[4] · Riadh Marzouki[5] · Sherif M. A. S. Keshk[6]

Received: 16 November 2023 / Accepted: 22 January 2024 / Published online: 1 March 2024

Abstract

Low-sulfonation-level polyether sulfone octyl sulfonamide (LSPSO) was blended with a layered double hydroxides (LDHs, Mg_2AlCl)/sepiolite nanostructure clay as a filler to create an electrolyte membrane for fuel cell applications. Comprehensive characterization of the composite membranes was conducted, encompassing Fourier-transform infrared spectroscopy, X-ray diffraction, mechanical stability assessment, thermal gravimetric analysis, ion exchange capability, swelling characteristics, water uptake performance, and electrochemical impedance spectroscopy analysis. In comparison to the pristine LSPSO membrane, the presence of LDHs/sepiolite nanoarchitecture material within LSPSO exhibited superior water retention and proton conductivity values, especially at elevated temperatures. The proton conductivity of the composite membranes reached approximately 250 mS/cm, while the unmodified LSPSO membrane only achieved 35 mS/cm at 100 °C. Moreover, LSPSO composite membranes demonstrated enhanced chemical and thermal stability along with higher proton conductivity when compared to pristine LSPSO membranes. These findings highlight the potential of developing tailored LSPSO composite membranes to advance the prospects of commercial applications in proton exchange membrane fuel cells.

Keywords Composite membrane · LSPSO · Layered double hydroxides · Sepiolite · Proton conductivity

Introduction

Extensive research has been undertaken to investigate the application of ion-exchange membranes within the context of proton exchange membrane fuel cells (PEMFCs). Aromatic polymers prove especially suitable for such purposes thanks to their favorable blend of exceptional thermal stability and ease of handling [1]. Utilizing the aromatic ring is frequently a top preference for alteration, resulting in the creation of polymers that display improved characteristics.

Polyether sulfone (PES), polybenzimidazole (PBI), and poly-aryl ether ketone (PEEK) are some examples of such polymers. Polyether sulfone (PES) stands out as an economical polymer commonly employed in the stage-reversal production of polymer films, serving purposes in microfiltration [2], ultrafiltration [3], gas separation [4], proton exchange membrane fuel cell [5], electrodialysis [6], modified electrode [7], and supercapacitors [8], thanks to its remarkable mechanical robustness and chemical durability [9]. However, it is important to note that PES possesses a significant hydrophobic nature, and one of the principal limitations associated

✉ Walid Mabrouk
w.mabroukcerte@gmail.com

1 Nanomaterials and Systems for Renewable Energy Laboratory, Research and Technology Center of Energy, Technoparc Borj Cedria, BP 095, Hammam Lif, Tunisia

2 Laboratory Water, Membranes and Environmental Biotechnology, Water Research and Technologies Center, Technologic Parc Borj Cedria, BP 273, 8020 Soliman, Tunisia

3 Ecochimie Laboratory, National Institute of Applied Sciences and Technology, University of Carthage, Tunis, Tunisia

4 Department of Chemistry, College of Science Al-Zulfi, Majmaah University, Al-Majmaah 11952, Saudi Arabia

5 Department of Chemistry, College of Science, King Khalid University, P.O. Box 9004, Abha 61413, Saudi Arabia

6 Become: Deep Tech & Nanoscience, 63 Rue de Tolbiac, 75013 Paris, France

with the PES layer is its susceptibility to membrane fouling [10]. Chemical modification of PES represents a primary strategy for enhancing the hydrophilicity and anti-fouling characteristics of PES membranes. Research has explored the synthesis and characterization of sulfonated polyether ketone or sulfonated poly sulfone (SPES) and PES polymer composites [11]. SPES exhibits favorable characteristics that satisfy all the necessary requirements for its application in an ideal PEMFC. However, it is worth noting that, like PES, SPES also presents certain drawbacks. Desirable traits for polymer composites include a strong elastic modulus, excellent proton conductivity properties, and endurance [12]. Various forms of SPES can be created by introducing octylamine into the SPES structure in different proportions, resulting in the formation of SPESOS [13]. SPESOS, owing to its lack of solubility in water, results in membranes that display fragility and showcase an extensive spectrum of ionic conductance and water uptake, contingent on the extent of octylamine grafting. There exist numerous approaches to augment both the mechanical attributes and ionic conductive characteristics of SPESOS-based membranes. SPESOS have less hydrophilic segments at the same ion exchange capacity (IEC) level as typical sulfonated ones, but they have more hydrophobic segments, which gives them good dimensional stability and mechanical qualities. The large polarity difference between the densely sulfonated, hydrophilic, and hydrophobic portions of the polymer was expected to result in greater microphase separation, which would lead to well-developed hydrophilic channels and higher proton conduction. Thus, the novel strategy for strengthening well-structured SPESOS is to use clays to create additional hydrophilic channels in it. Significantly, anionic clays known as layered double hydroxides (LDHs; $[M1\text{-}x^{2+}\ Mx^{3+}(OH)_2]x^{+}[(A^{-})_{x/n}\ yH_2O]$) have recently exhibited notable proton conductivity [14–16]. Surface –OH groups within the LDHs layer assume a vital function in aiding the dissociation of protons and their migration from one water molecule to the initial OH^{-} group, thereby leading to the creation of a notably elevated concentration of OH^{-} or H^{+} ions within the membrane [17]. In contrast, sepiolite, a naturally found hydrated mineral composed of ($[Si_{12}O_{30}\ Mg_8(OH,\ F)_4]\ (H_2O)_4{\cdot}8H_2O$), possesses a significant surface area and impressive adsorption capabilities, primarily owing to its porosity and the presence of silanol groups on the clay fibers. These features make it highly conducive to the adsorption of significant quantities of substances [18]. SPESOS is a densely sulfonated polymer that is gaining interest because of the large polarity difference between hydrophilic and hydrophobic units, which favors the creation of hydrophilic-hydrophobic phase-separated structures. These studies focused solely on the incorporation of clays with a high sulfonated SPESOS [19–25]. Recent research found that incorporating Hectorite clay onto low-sulfonated polyether sulfone octyl sulfonamide (LSPSO) resulted in a significant improvement in proton conductivity, attaining a fourfold increase (141.66 mS/cm) compared to the LSPSO membrane in isolation (35.04 mS/cm) [22]. In this regard, the goal of this study was to formulate a novel sort of composite using the LSPSO matrix and LDHs/sepiolite to improve moisture retention and ion transport capabilities inside the LSPSO layers. To accomplish this, various LDHs/sepiolite loading ratios were used in the production of LDHs/sepiolite /LSPSO composite membranes, which were then structural and morphologically assessed. A comprehensive assessment of the thermal stability, water retention capacity, and proton conductivity of a proton-conductive polymer composite will be performed. This novel composite has applications in a variety of fields, including electric chemical detectors, heat transmitters, and related domains.

Experimental

Resources

A lower sulfonated polyether sulfone derivative known as LSPSO was synthetized at the Eras Labo facility. *N*,*N*′-dimethylacetamide (DMAc) was acquired through Acros. Sulfuric acid was sourced from Scharlau, and sodium hydroxide was obtained from Laurylab.

Layered double hydroxides (LDHs)

LDHs were synthesized using the co-precipitation method [15]. Specifically, $MgCl_2{\cdot}6H_2O$ (0.66 M) and $AlCl_3{\cdot}6H_2O$ (0.33 M) were gradually introduced into a sodium hydroxide (NaOH) solution (100 mL, 1 M).

Simultaneously, a 2 M NaOH solution was continuously introduced under a nitrogen atmosphere to maintain a pH of 9.0 and minimize contamination from atmospheric CO_2. The resulting mixture was allowed to stand undisturbed for 24 h, after which the LDH (Mg_2AlCl) was collected through centrifugation and washed with deionized water.

Preparation of low sulfonated membrane

During the fabrication process of the low sulfonated polyether sulfone octyl sulfonamide (LSPSO) membrane, 1 g of LSPSO powder was dissolved in dimethylacetamide (DMAc), undergoing continuous magnetic stirring at room temperature for a duration of 15 min (refer to Fig. 1).

This process yielded a transparent and uniform polymer solution containing 10% by mass of LSPSO. Following that, the polymer solution was uniformly spread onto a Petri dish and exposed to drying under distinct conditions: 50 °C for 12 h, 80 °C for 6 h, and 100 °C for 12 h. After cooling, the

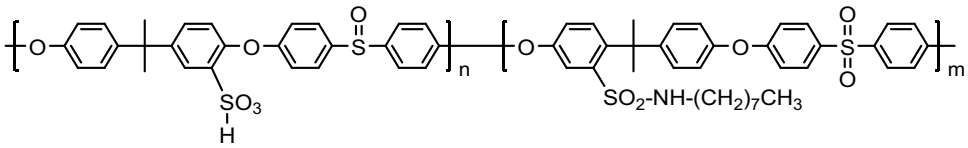

Fig. 1 Chemical structure of low sulfonated polyether sulfone octyl sulfonamide

LSPSO membrane was moistened using distilled water and carefully separated from the Petri dish. The resultant membrane was preserved within a moisture-rich setting for later utilization.

Preparation of LDHs/sepiolite nano-architecture material

The LDHs/sepiolite nanoarchitecture material was synthesized through a co-precipitation process, where LDH was precipitated in the presence of sepiolite to achieve a final nanostructured material with an equal weight ratio of one [12, 15, 23].

Preparation of composite membranes (LDHs/sepiolite/LSPSO)

Composite membranes were fabricated through a process that involved dispersing a solution, followed by a casting method and subsequent evaporation. Dispersion preparations involved mixing different quantities of LDHs/Sepiolite (1%, 3%, and 6% by mass) with LSPSO (10% by mass). In the beginning, LDHs/sepiolite powder was introduced into 5 mL of DMAc and stirred using a magnetic stirrer at ambient conditions. The resulting solutions were subjected to a 4-h ultrasonication process to ensure the uniform dispersion of the filler material.

Following this, each ratio of LDHs/sepiolite powder was introduced into the LSPSO solution. The resulting composite solutions underwent magnetic stirring for 2 h to facilitate thorough blending. The dispersion solutions were uniformly applied to a Petri dish support with a 20 cm^2 surface area, ensuring an even distribution of the samples across the support. Afterward, the membranes underwent the same drying process used for the reference LSPSO membrane under various conditions. Membranes were engineered to maintain a uniform thickness of approximately 100 µm across all samples.

Membrane characterization

Fourier transform infrared (FT-IR) analysis was performed in transmission mode with the utilization of an IR200 FT-IR spectrophotometer by Nicolet. Spectral data for both LSPSO and the diverse composite membranes were captured across the 400–4000 cm^{-1} range. To record the spectra, membrane specimens were positioned between the cast iron and the diamond crystal (separator blade) without undergoing prior treatment [24]. This approach enabled the precise characterization of membrane properties and analysis of the functional groups present.

X-ray diffraction examination was conducted with the automated system known as Bruker D8 Advance. Diffractograms of the dry composite membrane samples were acquired in the 2θ range spanning from 5° to 60°, and no pre-treatment was administered to the samples before analysis. The X-ray diffraction assessment enabled the examination of the crystal structure in both LSPSO and the associated composites [25]. The dimensions of the crystals in the materials were calculated employing the Scherrer equation, which is formulated as follows:

$$D = (\kappa\lambda/\beta D \times \cos\theta). \quad (1)$$

In this equation, D represents the size of the crystals in nanometers, λ signifies the radiation wavelength (specifically, 1.54056 Å for CuKα radiation), κ is a constant characterized by a value of 0.94, βD corresponds to the peak width at half-maximum intensity, and θ denotes the peak position. This analysis yielded valuable insights into the structural characteristics of the materials under investigation.

Thermogravimetric analysis (TGA) was conducted using a Mettle TGA instrument. Prior to analysis, the membrane specimens, with weights measuring around 2.5 and 3.5 mg, were subjected to a 24-h drying procedure at 100 °C to eliminate any lingering moisture and solvents. The TGA software was configured to elevate the temperature starting at 25 °C and reaching up to 900 °C, at a pace of 10 °C per minute, while sustaining a continuous nitrogen flow at a rate of 40 mL/min throughout the analysis. The TGA methodology facilitated the evaluation of both the thermal resilience and degradation patterns exhibited by the membrane specimens across an extensive span of temperatures [26].

The Hitachi 4800 II scanning electron microscope (SEM) was employed for sample observation, and no prior surface or cross-sectional treatment was administered before conducting the examinations [27]. This approach enabled the direct and unadulterated visualization of the membrane's structure and surface attributes at a remarkably high level of detail.

To assess the water uptake capacity (WU) of the membranes, we employed dry samples. The measurement of water uptake involved immersing each membrane in deionized water at room temperature for a duration of 72 h.

Afterward, any remaining surface moisture was meticulously removed using hydrophilic paper, and the weight of the membranes after this process was recorded. Water uptake (WU) values were then determined by calculating the relative increase in weight per gram of the initial dry specimen [28]. This calculation was performed by subtracting the weight of the sample before water absorption from its weight after water uptake. We applied Eq. (2) to derive the water uptake (WU) values.

$$\mathrm{WU} = \frac{W_{\mathrm{wet}} - W_{\mathrm{dry}}}{W_{\mathrm{dry}}} \times 100. \tag{2}$$

In this context, W_{wet} denotes the weight of the dampened membranes, whereas W_{dry} indicates the weight of the membranes when dry.

The contact angle (CA) of the various membranes was assessed using a Theta optical tensiometer. A precise droplet measuring 5 µL of demineralized water was gently deposited onto the membrane's surface, and an image of the droplet was captured using photographic equipment [29]. Subsequently, the software named Theta was employed to calculate the contact angle by analyzing the captured droplet image and determining the angle formed between the droplet and the surface of the membrane.

Ionic exchange capacity (IEC) determination was accomplished through an acid–base titration method. Each membrane, measuring 5×5 cm^2 in size, was individually soaked in a 100 mL aqueous solution containing sodium hydroxide (10^{-2} M) for a period of two days. Over this period, the sulfonated groups (SO_3H) within the membranes underwent conversion into sulfonate groups (SO_3Na) through an ion exchange mechanism. The protons released from the sulfonated groups were then countered by hydroxide ions (OH^-) within the solution, resulting in the formation of water. During the IEC calculation, titration procedures were carried out on both the starting solution and the sodium hydroxide (NaOH) solution using solutions of aqueous sulfonic acid. The amount of acid required to reach the titration endpoint was utilized to ascertain the concentration of the sodium hydroxide solution that reacted with the sulfonated groups within the membrane [30]. Following that, the IEC for each membrane was calculated using the subsequent correlation:

$$\mathrm{IEC} = \frac{n^i_{\mathrm{NaOH}} - n^f_{\mathrm{NaOH}}}{W_{\mathrm{dry}}} \tag{3}$$

In this equation, n^i_{NaOH} signifies the initial moles of sodium hydroxide within the solution (10^{-2} M, 200 mL), n^f_{NaOH} represents the moles of sodium hydroxide after the exchange, and W_{dry} indicates the mass of the membrane when dry.

The sulfonation degree (DS) for LSPSO was calculated by employing the formula based on ion exchange capacity values [12, 24, 31]:

$$\mathrm{DS}(\%) = \frac{M_2 \times \mathrm{IEC}}{1000 + \left(M_2 - M_1\right) \times \mathrm{IEC}} \tag{4}$$

where M_1 stands for the molar mass of LSPSO (505.53 g/mol) and M_2 corresponds to the molar mass of PES (442.53 g/mol).

Proton conductance assessments in the membranes were carried out via the utilization of Electrochemical Impedance Spectroscopy (EIS) utilizing a VSP potentiostat from Biologic Science Instruments. Samples cut as circles with a diameter of 1 cm were placed in a cell provided by a temperature controller and were clamped between two golden stainless-steel blocking electrodes. The EIS measurements were performed under 100% relative humidity (RH), varying the temperature.

Electrical resistance (R) for each membrane was determined by identifying the intersection point of the high-frequency Nyquist plots with the x-axis [32, 33]. To calculate ionic conductance (σ, mS/cm), the following equation was utilized:

$$\sigma(\mathrm{mS/cm}) = \frac{e}{R \times S} \tag{5}$$

Here, 'e' represents the thickness of the membrane, 'S' denotes the surface area of the membrane situated between the two electrodes, and 'R' stands for the electrical resistance.

Results and discussion

The uniform dispersion of organic and clay components became apparent through the composite membrane's considerable thickness, its see-through appearance, and its pale ivory coloration (Fig. 2). The surface area of the clay (144 m^2/g) was sufficient to host the LSPSO with a sulfonation level of 0.9 protons per monomer unit [13]. Furthermore, a highly effective hybrid material was produced through robust interfacial interactions between clay and an aromatic polymer matrix. This phenomenon can be elucidated by the establishment of non-covalent connections, facilitated by hydrogen bonding interactions between the SO_3H groups within LSPSO chains and the basal planes of the clay, as will be demonstrated via FTIR and XRD analyses.

Fourier transform infrared spectroscopy

Figure 3 displays FT-IR spectra spanning the 500–2000 cm^{-1} range, encompassing LSPSO as well as films with various clay ratio/LSPSO compositions.

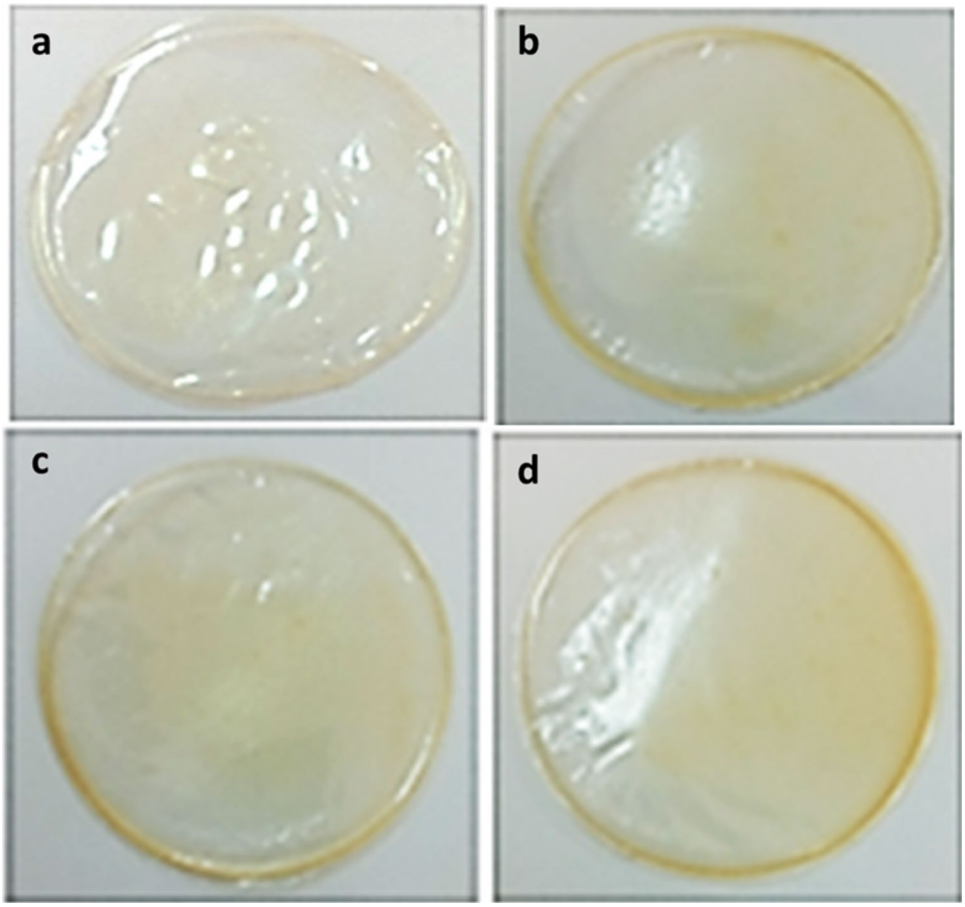

Fig. 2 Photo of the various membranes. **a** LSPSO, **b** 1 wt% LDHs-Sep/LSPSO, **c** 3 wt% LDHs-Sep/LSPSO and **d** 6 wt% LDHs-Sep/LSPSO

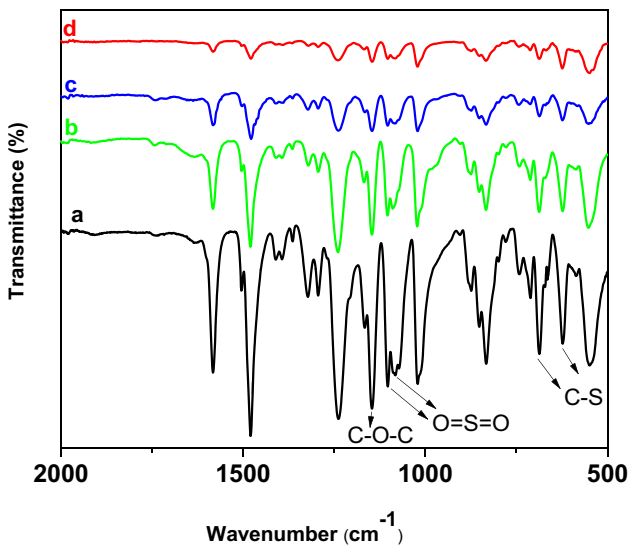

Fig. 3 FT-IR spectra of (a) LSPSO, (b) 1wt% LDHs-Sep/LSPSO, (c) 3wt% LDHs-Sep/LSPSO and (d) 6 wt% LDHs-Sep/LSPSO composite membranes

Due to the constrained clay content in LSPSO, the spectral profiles of the different composite membranes exhibit noteworthy resemblance. The FT-IR spectra reveal two prominent peaks at 1480 and 1584 cm^{-1}, serving as markers for the presence of aromatic carbons. Furthermore, a band at 1240 cm^{-1} confirms the presence of a methyl group within LSPSO. The identification of the C–O–C group is apparent due to the peak detected at 1150 cm^{-1}. The symmetrical and asymmetrical stretching vibrations of the O=S=O group are distinguishable by the characteristic bands observed at 1105 and 1082 cm^{-1}, respectively. Furthermore, the presence of C–S groups is accountable for the bands observed at 688 and 625 cm^{-1} [19]. The FTIR spectra obtained from the composite membranes closely mirrored those of the LSPSO membrane, showing no substantial differences.

This implies that there is no evidence of a chemical reaction occurring between the clay and LSPSO. Simultaneously, the asymmetric and symmetric vibrations linked to O=S=O at 1105 and 1082 cm^{-1}, in addition to the two characteristic LSPSO bands connected to aromatic carbons at 1480 and 1584 cm^{-1}, displayed a reduction in intensity within the hybrid films (refer to Fig. 3). These findings indicate a lack of covalent bonding or stacking interactions between

the phenyl groups within LSPSO chains, SO_3H groups, and the clay's basal planes.

X-ray diffractograms

In Fig. 4, you can observe the diffractograms for composite membranes containing clay and LSPSO, showcasing various clay ratios.

The primary peak of LSPSO at $2\theta = 14.6°$, corresponding to the (001) plane, signified a significant alteration in the LSPSO membrane.

The introduction of clay induced favorable macromolecular orientations of the polymer chains, causing a shift in the dominant peak of the LSPSO composite towards a lower 2θ value. The presence of clay created compressive stress and a difference in ionic radii between LSPSO and the dopant ion (clay), resulting in expansion. Consequently, the peaks in the composite membranes shifted towards lower angles, accompanied by an increase in the inter-planar distance (d) and an expansion of the host lattice (Table 1).

The diffraction plane of LSPSO composites exhibited a noticeable shift towards lower angles (from 12.72° to 13.40°) as clay was incorporated into the LSPSO matrix, particularly concerning the (001) plane, which aligns parallel to the surface. This shift in peak positions in the composite can be attributed to an increased atomic spacing within the composite, resulting in a rise in the average lattice parameter. This occurrence can be credited to the dispersion of clay nanoparticles by the LSPSO chains, aided by ionic interactions involving the sulfonic groups within LSPSO and the ions present on the clay's surface. These observations are consistent with the investigations carried out by Charradi et al. [12, 15]. The rise in the interplanar distance observed in the LSPSO composites, expanding from 6.35 to 7.04 Å, is indicative of the intercalation of clay layers by monolayers and/or multilayers of LSPSO chains. Additionally, there was a significant increase in the crystallite size of the composite when compared to the pristine LSPSO (refer to Table 1).

Table 1 XRD analysis of LSPSO and LDH-Sep/LSPSO composite membranes

Sample	2θ (°)	d (001) Å	Crystallite size (nm)
LSPSO	14.10	6.35	11.37
1 wt% LDHs-Sep/LSPSO	13.40	6.68	20.94
3 wt% LDHs-Sep/LSPSO	13.27	6.75	25.75
6 wt% LDHs-Sep/LSPSO	12.72	7.04	25.73

Contact angle

This can be attributed to the influence of clay, which potentially impacts the aggregation of LSPSO particles through mechanisms such as grain-boundary pinning effects or alterations in surface energy and charge distribution [26]. The alterations in the surface properties of LSPSO resulting from the LDH-Sep inclusion process can be elucidated through the utilization of drop shape analysis, as depicted in Fig. 5.

The analysis of contact angles provides valuable insights into the exceptional wetting properties of the composite components. By examining contact angles across various membranes, we can effectively compare the super-wettability of LSPSO with its composite counterparts. The initial contact angle for the pristine LSPSO membrane measures 87.54°. However, with the incorporation of clay into the composite membranes at concentrations of 1 wt%, 3 wt%, and 6 wt%, the contact angle consistently diminishes to values of 75.79°, 69.97°, and 57.71°, as depicted in Fig. 5. The decrease in the contact angle, which can be attributed to the presence of clay, indicates an increase in hydrophilicity. It's crucial to bear in mind that reduced contact angles in flat sheet membranes signify enhanced hydrophilic characteristics [15, 16, 19, 25]. Hence, the measurements of contact angle indicate that the surfaces of the composite membranes possess enhanced wetting characteristics when compared to the individual constituent materials.

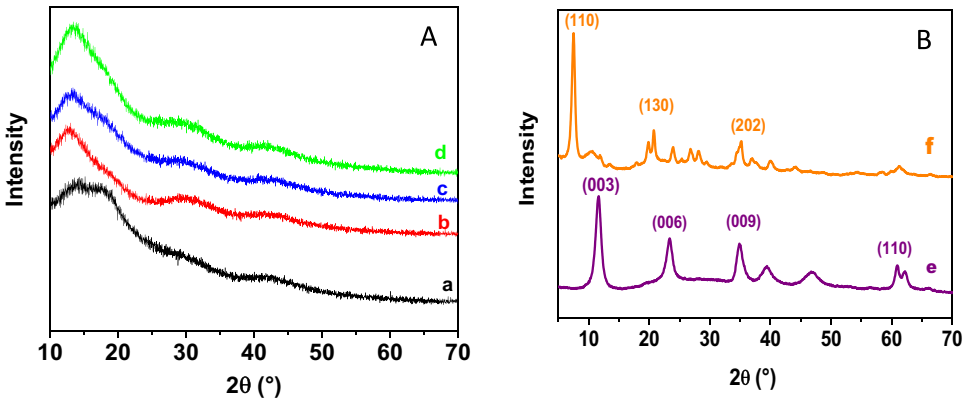

Fig. 4 X-ray diffraction patterns **A**: (a) LSPSO, (b) 1 wt% LDHs-Sep/LSPSO, (c) 3 wt% LDHs-Sep/LSPSO and (d) 6 wt% LDHs-Sep/LSPSO composite membranes, **B** (e) LDHs and (f) LDHs/Sepiolite

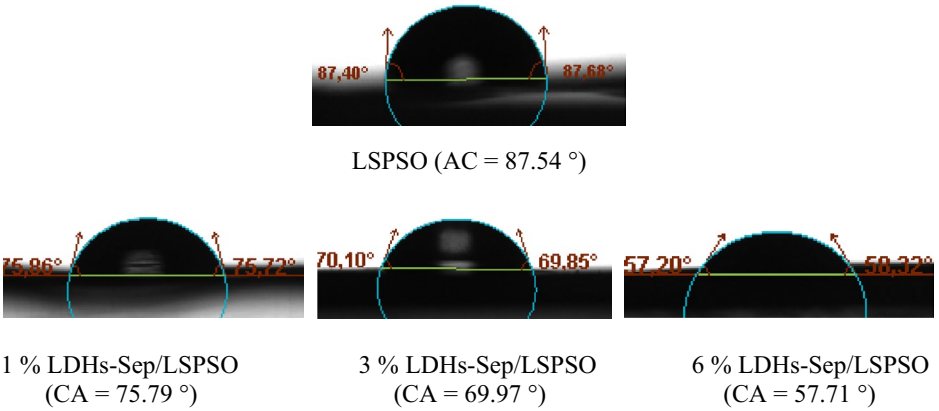

Fig. 5 Contact angle of fabricated composite membranes

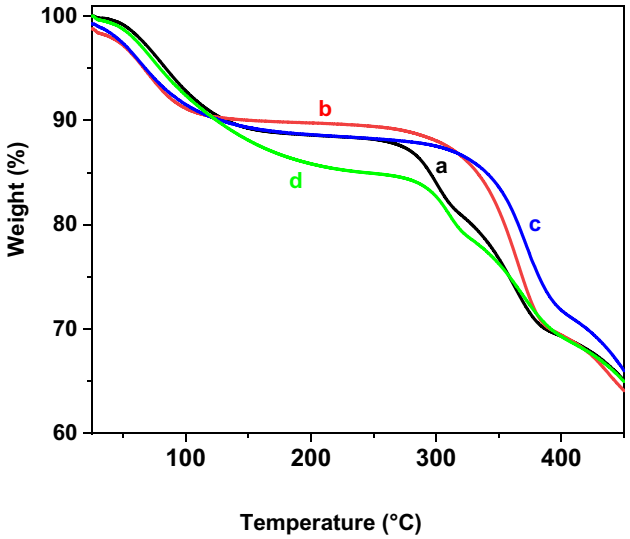

Fig. 6 Thermogravimetric analysis of (a) LSPSO (b) 1 wt% LDHs-Sep/LSPSO, (c) 3 wt% LDHs-Sep/LSPSO and (d) 6 wt% LDHs-Sep/LSPSO composite membranes

Thermogravimetric analysis

In the thermogravimetric analysis (TGA) of the various fabricated membranes, we observe a generally consistent behavior across the different membranes, without any notable deviations, as depicted in Fig. 6.

During thermal analysis, it's notable that all membranes exhibit a triphasic weight loss pattern. The initial phase of mass decrease transpires at around 100 °C and can be attributed to the vaporization of moisture within the LSPSO matrix. Following that, a significant secondary mass reduction, which takes place approximately at 300 °C, indicates the potential degradation of sulfonic groups. Finally, a subsequent mass reduction is observable around 470 °C, indicating the degradation of the primary polymer matrix. Upon comparing the thermogravimetric analysis (TGA) outcomes of the LSPSO membrane with those of all LSPSO composite membranes, no substantial disparities in decomposition characteristics are discernible throughout the entire investigated temperature range. However, in TGA curves depicting the composite membranes, a conspicuous trend towards higher temperatures is observed when clay is integrated into LSPSO at concentrations of 1 wt% and 3 wt%. In a comparative analysis between the composite membranes and the LSPSO membrane, a comprehensive examination of the TGA curves reveals that the composite membranes exhibit an increased capacity for water retention. Notably, the incorporation of clay at a concentration of 6 wt% results in the most significant water loss, totaling 15%. This occurs because of a higher concentration of clay within the membrane, resulting in increased water content within the composite. [12, 15, 19]. In contrast, the composite membranes with 1 wt% and 3 wt% clay display water losses of roughly 8 wt% and 10 wt%, respectively.

Table 2 Ion exchange capacity and degree of sulfonation of various membranes

Sample	IEC (meq/g)	DS (%)
LSPSO	1.80	71.53
1 wt% LDHs-Sep/LSPSO	1.81	71.89
3 wt% LDHs-Sep/LSPSO	1.78	70.82
6 wt% LDHs-Sep/LSPSO	1.82	72.25

Ion exchange capacity and degree of sulfonation

Table 2 compiles the values of ion exchange capacity and sulfonation degree for all prepared membranes.

Regarding the measurements of ion exchange capacity (IEC), which were established through acid–base titration across the various membrane preparations, they consistently reside within the range of approximately 1.8 milliequivalents per gram (meq/g). As the presence of inert clay within the

LSPSO matrix does not influence this measure, these outcomes consistently align with the composition of LSPSO. To assess the achieved sulfonation degree of LSPSO and its composites, we used Eq. 4. The sulfonation degree of all composite membrane was approximately 71% similar to that of LSPSO membrane does not alter this property, as the clay nanoparticles do not contain sulfonic groups in their structure.

Water uptake

Furthermore, it was established that the LSPSO material employed exhibited an 71% sulfonation level. In Fig. 7, the fluctuations in water uptake, computed via Eq. 1, for all composite membranes are juxtaposed with that of LSPSO (1.8 meq/g).

In Fig. 7, the graphic representation portrays the connection between the clay content in both LSPSO membranes and composite membranes, along with their corresponding water absorption properties. When comparing the composite membranes with the unaltered LSPSO membranes (exhibiting a water uptake of 37%), it becomes evident that the composite membranes exhibit superior water-absorbing capabilities. The innate hydrophilicity of clay, a vital factor contributing to improved water uptake, collaborates with the sulfonic groups within the LSPSO polymer, thereby leading to the observed augmentation in water absorption. Figure 7 effectively illustrates the correlation between the clay content in both LSPSO and composite membranes and their respective water absorption capacities. The inherent hydrophilic nature of clay, a critical factor in enhancing water absorption, collaborates with the sulfonic groups present in the LSPSO polymer, contributing to the observed rise in water uptake. The introduction of clay can alter the size of LSPSO particles and induce clustering, potentially leading to modifications in the microstructure of LSPSO. The increase in the rate of water absorption can be ascribed to the incorporation of clay into the LSPSO matrix, which leads to an expansion in the overall volume and the creation of solvated proton transport pathways [34–37].

Proton conductivity

To evaluate the electrochemical performance of the membrane, AC impedance spectroscopy was employed to assess its ability to facilitate proton migration. These evaluations were carried out within a temperature range spanning from room temperature to 100 °C, with a relative humidity (RH) of 100%, as illustrated in Fig. 8.

In all temperature ranges, a consistent observation was the lower proton conductivity exhibited by the LSPSO reference membrane. At a temperature of 100 °C, the proton conductivity of LSPSO was recorded at 35 mS/cm. In contrast, the nanocomposite membranes, which incorporated clay at concentrations of 1 wt%, 3 wt%, and 6 wt% by weight, exhibited significantly higher proton conductivities, measuring 128 mS/cm, 167 mS/cm, and 251 mS/cm, respectively. The substantial improvement in proton conductivity can be attributed to the abundant presence of ions within the clay. These ions create stronger electrostatic fields that can better accommodate water molecules. This, in turn, facilitates the formation of a denser and more extensive hydrogen-bonding network, thereby enhancing proton transport. The observed

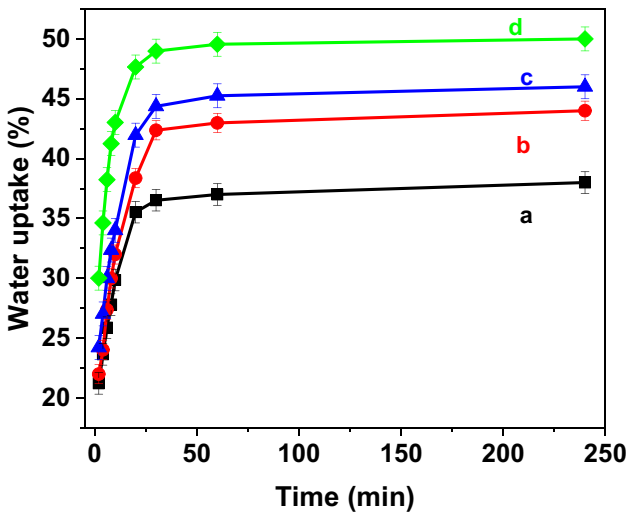

Fig. 7 Water uptake statistics of the composite membrane with increasing LDHs-Sep percentage in pristine LSPSO membrane (a) LSPSO, (b) 1 wt% LDHs-Sep/LSPSO, (c) 3 wt% LDH-Sep/LSPSO and (d) 6 wt% LDHs-Sep/LSPSO composite membranes

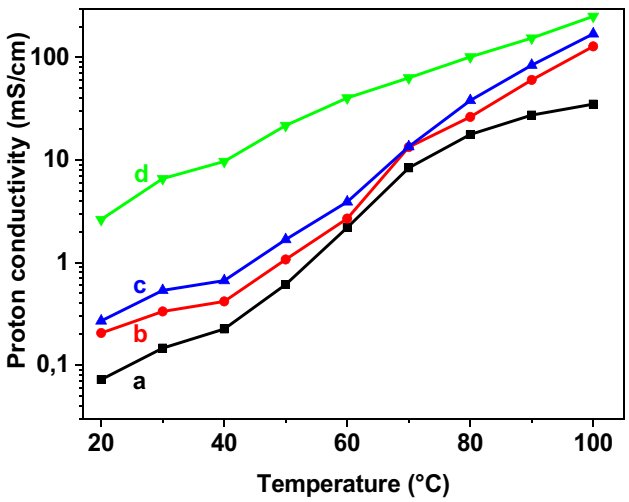

Fig. 8 Evolution of proton conductivity of different composite membranes at 100% relative humidity (a) LSPSO, (b) 1 wt% LDHs-Sep/LSPSO, (c) 3 wt% LDHs-Sep/LSPSO and (d) 6 wt% LDHs-Sep/LSPSO composite membranes

Table 3 Activation energy values and proton conductivity at 100 °C

Membrane	Conductivity (mS/cm) at 100 °C	E_a (kJ/mol)
LSPSO	35.04	100
1 % LDHs-Sep/LSPSO	128.12	95
3 % LDHs-Sep/LSPSO	169.93	93
6 % LDHs-Sep/LSPSO	251.40	65

improvement in proton conductivity across the composite membranes, featuring different clay concentrations, may be attributed to the heightened ability of protons to solvate in water at elevated temperatures (100 °C). It's important to highlight that as the clay percentage increases, the proton conductivity of composite membranes consistently shows an upward trend. The layered structure and hygroscopic nature of clay provide advantages for enhancing water retention, especially under high-temperature conditions. Incorporating LDH/Sepiolite into the LSPSO matrix significantly elevates proton conductivity to 251 mS/cm at 100 °C, marking a substantial enhancement compared to LSPSO containing Hectorite, which measured 141 mS/cm under identical test conditions and clay concentration [22]. To elucidate the correlation between temperature and proton conductivity, one can utilize the Arrhenius equation. As a result, you can employ the subsequent equation to compute the activation energy for conductivity:

$$\sigma = \sigma_0 \exp(-E_a/RT) \tag{6}$$

In the provided equation, σ signifies proton conductivity in S/cm, σ_0 represents the pre-exponential factor, R is the universal gas constant (8.314472 J/mol K), and T stands for the absolute temperature in Kelvin (K). The activation energies for LSPSO, computed using Eq. 4, are presented in Table 2. Moreover, the activation energies of the nanocomposite membranes are also provided, as determined through experiments conducted at 100% relative humidity (RH).

Under experimental conditions maintained at 100% relative humidity (RH), the activation energy for both composite and LSPSO membranes was assessed, and the outcomes are detailed in Table 3. It is evident that the composite membranes exhibit lower activation energy values in comparison to membranes composed solely of unaltered LSPSO [19, 22, 25, 36]. The presence of the filler material exerts a notable influence on the activation energy, with the lowest value observed in the composite membrane containing 6% clay. This observation further substantiates previous findings that the composite membranes exhibit enhanced proton conductivity. The inclusion of nanofillers in membranes promotes the retention of water absorbed within the polymer, a decrease of E_a from 100 to 65 kJ/mol for LSPSO and 6% LDHs-Sep LSPSO thereby enhancing proton conductivity can be through vehicular and Grothus mechanisms.

Consequently, the heightened proton conductivity observed with the augmented presence of inorganic fillers indicates an improved pathway for proton movement due to increased water uptake. Vehicular mechanisms, the activation energy (E_a) achieved for Nafion membranes in the presence of clay is notably low [35, 38–40]. In fact, the Grottuss mechanism dominates in the proton conduction, the activation should be more important like SPEEK membrane in the presence of clay [12, 15]. In fact, both mechanisms can be active, making it challenging to pinpoint the predominant one. Proton conductivity experiences enhancement when the filler interacts with the sulfonic groups, serving not only to absorb water molecules but also to act as an active site that facilitates proton transport.

Conclusion and future outlook

The effective integration of LDHs sepiolite into the LSPSO matrix was confirmed through FT-IR and XRD analyses. Furthermore, investigations included crucial parameters, including water absorption and proton conductivity. The impressive performance demonstrated by the composite membranes highlights their appropriateness for electrochemical applications. Unlike the unmodified LSPSO membranes, the composite membranes exhibit remarkable stability even when exposed to temperatures as high as 100 °C, while also maintaining strong proton conductivity. This confirms that the incorporation of clay improves membrane stability and water absorption capacity.

Acknowledgements The authors extend their gratitude to the manager of Eras Labo (Saint-Nazaire-Les-Eymes, France) for generously supplying the Low Sulfonated Polyether Sulfone Octyl Sulfonamide (LSPSO) polymer free charge.

Author contributions KC formal analysis, investigation, methodology, writing original draft, writing-review and editing; WM data curation, measurements, formal analysis, investigation, writing-original draft, writing-review and editing; IBK and YA-G investigation, measurements, resources, data curation, formal analysis, visualization; NB validation, visualization, writing original draft; RM data curation, investigation, funding acquisition, writing original draft; SMASK conceptualization, writing review and editing, visualization, supervision, funding acquisition.

Data availability Data will be available on request.

Declarations

Conflict of interest The authors declare that they have no conflict of interest.

Author information The manuscript was written through the contributions of all authors. All authors have given approval to the final version of the manuscript.

References

1. Hooshyari, K., Rezania, H., Vatanpour, V., Salarizadeh, P., Askrai, M.B., Beydaghi, H., Enhessari, M.: High temperature membranes based on PBI/sulfonated polyimide and doped-perovskite nanoparticles for PEM fuel cells. J. Membr. Sci.Membr. Sci. **612**, 118436 (2020). https://doi.org/10.1016/j.cej.2013.02.130
2. Liu, S., Edara, P.C., Schäfer, A.I.: Influence of organic matter on the photocatalytic degradation of steroid hormones by TiO_2-coated polyethersulfone microfiltration membrane. Water Res. **245**, 120438 (2023). https://doi.org/10.1016/j.waters.2023.120438
3. Turgut, F., Chong, C.Y., Karaman, M., Lau, W.J., Gürsoy, M., Ismail, A.F.: Plasma surface modification of graphene oxide nanosheets for the synthesis of GO/PES nanocomposite ultrafiltration membrane for enhanced oily separation. J. Appl. Polym. Sci.Polym. Sci. **140**, e53410 (2023). https://doi.org/10.1002/app.53410
4. Maleh, M.S., Kiani, S., Raisi, A.: Study of the advantageous effect of nano-clay polyurethane on structure and CO_2 separation performance of polyethersulfone based ternary mixed matrix membranes. Chem. Eng. Res. Design **179**, 27–40 (2022). https://doi.org/10.1016/j.cherd.2022.01.011
5. Mabrouk, W., Ogier, L., Vidal, S., Sollogoub, C., Matoussi, F., Dachraoui, M., et al.: Synthesis and characterization of polymer blends of sulfonated polyethersulfone and sulfonated polyethersulfone octylsulfonamide for PEMFC applications. Fuel Cells. **2**, 179–187 (2012). https://doi.org/10.1002/fuce.201100051
6. Mabrouk, W., Lafi, R., Fauvarque, J.F., Hafiane, A., Sollogoub, C.: New ion exchange membrane derived from sulfochlorated polyether sulfone for electrodialysis desalination of brackish water. Polym. Adv. Technol.. Adv. Technol. **32**, 304–314 (2021). https://doi.org/10.1002/pat.5086
7. Baachaoui, S., Mabrouk, W., Charradi, K., Slimi, B., Ramadan, A.M., Elsamra, R.M.I., Keshk, S.M.A.S., Raouafi, N.: Laser-induced porous graphene electrodes from polyketmine membranes for paracetamol sensing. R. Soc. Open. Sci. **10**, 230294 (2023). https://doi.org/10.1098/rsos.230294
8. Baachaoui, S., Mabrouk, W., Rabti, A., Ghodbane, O., Raouafi, N.: Laser-induced graphene electrodes scribed onto novel carbon black-doped polyethersulfone for flexible high-performance. J. Colloid Interface Sci. **646**, 1–10 (2023). https://doi.org/10.1016/j.jcis.2023.05.024
9. Rastegarpanah, A., Mortaheb, H.R.: Surface treatment of polyethersulfone membranes for applying in desalination by direct contact membrane distillation. Desalination **377**, 99–107 (2016). https://doi.org/10.1016/j.desal.2015.09.008
10. Ahmad, A.L., Abdulkarim, A.A., Ooi, B.S., Ismail, S.: Recent development in additives modifications of polyethersulfone membrane for flux enhancement. Chem. Eng. J. **223**, 246–267 (2013). https://doi.org/10.1016/j.cej.2013.02.130
11. Lau, W.J., Ismail, A.F.: Effect of SPEEK content on the morphological and electrical properties of PES/SPEEK blend nanofiltration membranes. Desalination **249**, 996–1005 (2009). https://doi.org/10.1016/j.desal.2009.09.016
12. Ahmed, Z., Charradi, K., Alsulami, Q.A., Keshk, S.M.A.S., Chtourou, R.: Physicochemical characterization of low sulfonated polyether ether ketone/smectite clay composite for proton exchange film fuel cells. J. Appl. Polym. Sci.Polym. Sci. **138**, 49634–49642 (2021). https://doi.org/10.1002/app.49634
13. Mabrouk, W., Ogier, L., Matoussi, F., Sollogoub, C., Vidal, S., Dachraoui, M., Fauvarque, J.F.: Preparation of new proton exchange membranes using sulfonated poly(ethersulfone) modified by octylamine (SPESOS). Mater. Chem. Phys. **128**, 456–463 (2011). https://doi.org/10.1016/j.matchemphys.2011.03.031
14. Wang, Y., Yan, D., El Hankari, S., Zou, Y., Wang, S.: Recent progress on layered double hydroxides and their derivatives for electrocatalytic water splitting. Adv. Sci. **5**, 1800064 (2018). https://doi.org/10.1002/advs.201800064
15. Charradi, K., Ahmed, Z., Thmaini, N., Aranda, P., Al-Ghamdi, Y.O., Ocon, P., Keshk, S.M.A.S., Chtourou, R.: Incorporating of layered double hydroxide/sepiolite to improve the performance of sulformance of sulfonated poly(ether ether ketone) composite membranes for proton exchange membrane fuel cells. J. Appl. Polym. Sci.Polym. Sci. **138**, 50364 (2021). https://doi.org/10.1002/app.50364
16. Charradi, K., Landolsi, Z., Gabriel, L., Mabrouk, W., Koschella, A., Ahmed, Z., Elnaggar, A., Heinze, T., Keshk, S.M.A.S.: Incorporating of sulfo ethyl cellulose to augment the performance of sulfonated poly (ether ether ketone) composite for proton exchange membrane fuel cells. J. Solid State Electron. (2023). https://doi.org/10.1007/s10008-023-05629-0
17. Hu, S., Lozada-Hidalgo, M., Wang, F.C., Mishchenko, A., Schedin, F., Nair, R.R., Hill, E.W., Boukhvalov, D.I., Katsnelson, M.I., Dryfe, R.A.W., Grigorieva, I.V., Wu, H.A., Geim, A.K.: Proton transport through one-atom-thick crystals. Nature **516**, 227–230 (2014). https://doi.org/10.1038/nature14015
18. Ma, J., Bilotti, E., Peijs, T., Darr, J.A.: Preparation of polypropylene/sepiolite nanocomposites using supercritical CO_2 assisted mixing. Eur. Polym. J.Polym. J. **43**, 4931–4939 (2007). https://doi.org/10.1016/j.eurpolymj.2007.09.010
19. Mabrouk, W., Charradi, K., Lafi, R., AlSalem, H.S., Maghraoui-Meherzi, H., Keshk, S.M.A.S.: Augmentation in proton conductivity of sulfonated polyether sulfone octyl sulfonamide using sepiolite clay. J. Mater. Sci. **57**, 15331–15339 (2022). https://doi.org/10.1007/s10853-022-07627-5
20. Mabrouk, W., Charradi, K., Mellekh, A., Hafiane, A., Alsulami, Q.A., Meherzi, H.M., Chtourou, R., Keshk, S.M.A.S.: Enhanced proton conductivity of sulfonated poly ether sulfone octyl sulfonamide membrane via the incorporation of protonated montmorillonite. J. Electron. Mater. **52**, 2158–2167 (2023). https://doi.org/10.1007/s11664-022-10183-y
21. Mabrouk, W., Charradi, K., Meherzi, H.M., Alhussein, A., Keshk, S.M.A.S.: Proton conductivity amelioration of sulfonated poly ether sulfone octyl sulfonamide via the incorporation of montmorillonite. J. Electron. Mater. **51**, 6369–6378 (2022). https://doi.org/10.1007/s11664-022-09862-7
22. Mabrouk W., Charradi, K., Ben Kacem, I., Lafi, R., Bellakhal, N., Marzouki, R., Keshk, S.M.A.S.: Significant augmentation of proton conductivity in low sulfonated polyether sulfone octyl sulfonamide membranes through the incorporation of hectorite clay. Mater. Renew. Sustain. Energy. https://doi.org/10.1007/s40243-023-00251-6
23. Charradi, K., Forano, C., Prevot, V., Madern, D., Ben Haj Amara, A., Mousty, C.: Characterization of hemoglobin immobilized in MgAl-layered double hydroxides by the coprecipitation method.

Langmuir **26**, 9997–10004 (2010). https://doi.org/10.1021/la1001286
24. Huang, R.Y.M., Shao, P., Burns, C.M., Feng, X.: Sulfonation of poly(ether ether ketone) (PEEK): kinetic study and characterization. J. Appl. Polym. Sci.Polym. Sci. **82**, 2651–2660 (2001). https://doi.org/10.1002/app.2118
25. Mabrouk, W., Jebri, S., Charradi, K., Silimi, B., Alzahrani, A.Y.A., Boubakri, A., Ghodbane, O., Raouafi, N., Keshk, S.M.A.S.: Fabrication and characterization of graphene/sulfonated polyether sulfone octyl sulfonamide hybrid film with improved proton conductivity performance. J. Solid State Electron. **27**, 991–999 (2023). https://doi.org/10.1007/s10008-023-05411-2
26. Ding, R., Hu, Y., Gui, Z., Zong, R., Chen, Z., Fan, W.: Preparation and characterization of polystyrene/graphite oxide nanocomposite by emulsion polymerization. Polym. Degrad. Stabil. **81**, 473–476 (2003). https://doi.org/10.1016/S0141-3910(03)00132-0
27. Mabrouk, W., Ogier, L., Sollogoub, C., Vidal, S., Matoussi, F., Fauvarque, J.F.: Synthesis and characterization of new membranes deriving from sulfonated polyethersulfone for PEMFC applications. Desalin. Water Treat.. Water Treat. **56**, 2637–2645 (2015). https://doi.org/10.1080/19443994.2015.1024939
28. Mabrouk, W., Lafi, R., Charradi, K., Ogier, L., Hafiane, A., Fauvarque, J.F., Sollogoub, C.: Synthesis and characterization of new proton exchange membrane deriving from sulfonated polyether sulfone using ionic crosslinking for electrodialysis applications. Polym. Eng. Sci.. Eng. Sci. **60**, 3149–3158 (2020). https://doi.org/10.1002/pen.25543
29. Mabrouk, W., Lafi, R., Hafiane, A.: Electrodialysis performance during the defluoridation of brackish water using ClNH2 membrane. Desalin. Water Treat.. Water Treat. **236**, 16–25 (2021). https://doi.org/10.5004/dwt.2021.27669
30. Dombaycioglu, S., Günsel, H., Aydin, A.O.: Nafion/Aquivion-based composite lithium ion exchange membranes for high capacity Li-S batteries. Chem. Sel. **7**, e202202910 (2022). https://doi.org/10.1002/slct.202202910
31. Bae, G.N., Kim, H.W., Jung, E.M., Kang, S., Shul, Y.G., Peck, D.H.: Effect on the electrochemical performance of surface-modified mordenite in a PTFE Nafion composite membrane for direct methanol fuel cells. Int. J. Hydrogen Energy **48**, 18879–18889 (2023). https://doi.org/10.1016/j.ijhydene.2023.02.001
32. Iriarte, D., Andrada, H., Ochoa, S.A.M., Silva, O.F., Chavez, F.V., Carreras, A.: Effect of acid treatment on the physic-chemical properties of Nafion 117 membrane. Int. J. Hydrogen Energy **47**, 21253–21260 (2022). https://doi.org/10.1016/j.ijhydene.2022.04.246
33. Dönmez, G., Gülcan, M., Deligöz, H.: A comparative study on sPEEK-based composite membranes with various inorganic fillers using different preparation routes for DMFCs. Polym. Eng. Sci.. Eng. Sci. **63**, 2920–2930 (2023). https://doi.org/10.1002/pen.26416
34. Verma, P., Daverey, A., Arunachalam, K.: Development and characterization of novel low-cost engineered pine needle biochar and montmorillonite clay based proton exchange membrane for microbial fuel cell. J. Water Process Eng. **53**, 103750 (2023). https://doi.org/10.1016/j.jwpe.2023.103750
35. Boulif, N., Evers, R., Houben, M., Borneman, Z., Nijmeiji, K.: Structure and performance of clay composite membranes with improved sodium conductivity for salinity gradient batteries. Appl. Clay Sci. **245**, 107136 (2023). https://doi.org/10.1016/j.clay.2023.107136
36. Hus, W.Y., Gierke, T.D.: Ion transport and clustering in nafion perfluorinated membranes. J. Membr. Sci.Membr. Sci. **13**, 307–326 (1983). https://doi.org/10.1016/S0376-7388(00)81563-X
37. Li, J.Y., Nasser, S.N.: Micromechanical analysis of ionic clustering in Nafion perfluorinated membrane. Mech. Mater. **32**, 303–314 (2000). https://doi.org/10.1016/S0167-6636(00)00002-8
38. Charradi, K., Ahmed, Z., Escudero Cid, R., Aranda, P., Ruiz-Hitzky, E., Ocon, P., Chtourou, R.: Amelioration of PEMFC performance at high temperature by incorporation of nanofiller (sepiolite/layered double hydroxide) in Nafion membrane. Int. J. Hydrogen Energy **44**, 10666–10676 (2019). https://doi.org/10.1016/j.ijhydene.2019.02.183
39. Thmaini, N., Charradi, K., Ahmed, Z., Chtourou, R., Aranda, P.: Nanoarchitectonics of fibrous clays as fillers of improved proton-conducting membranes for fuel-cell applications. Appl. Clay Sci. **242**, 107019 (2023). https://doi.org/10.1016/j.clay.2023.107019
40. Thmaini, N., Charradi, K., Ahmed, Z., Aranda, P., Chtourou, R.: Nafion/SiO2@TiO2-palygorskite membranes with improved proton conductivity. J. Appl. Polym. Sci.Polym. Sci. **139**, 52208 (2022). https://doi.org/10.1002/app.52208